Optics Communications 382 (2017) 18–27

Contents lists available at ScienceDirect

Optics Communications

journal homepage: www.elsevier.com/locate/optcom

Fast three-dimensional measurements for dynamic scenes with shiny surfaces

Shijie Feng [a,b,c,*], Qian Chen [a], Chao Zuo [a,b], Anand Asundi [c]

[a] Jiangsu Key Laboratory of Spectral Imaging & Intelligent Sense, Nanjing University of Science and Technology, Nanjing, Jiangsu Province 210094, China
[b] Smart Computational Imaging Laboratory (SCILab), Nanjing University of Science and Technology, Nanjing, Jiangsu Province 210094, China
[c] Centre for Optical and Laser Engineering, School of Mechanical and Aerospace Engineering, Nanyang Technological University, Singapore 639798, Singapore

ARTICLE INFO

Article history:
Received 20 May 2016
Received in revised form
20 July 2016
Accepted 21 July 2016

Keywords:
Fast three-dimensional measurements
Shiny surfaces
Fringe projection
Dynamic scenes
Stereo
Digital speckle

ABSTRACT

This paper presents a novel fringe projection technique for fast three-dimensional (3-D) shape measurements of moving highly reflective objects. By combining the standard three-step phase-shifting fringe patterns with a digital speckle image, dynamic 3-D reconstructions of shiny surfaces can be efficiently achieved with only four projected patterns. The phase measurement is performed by three-step phase-shifting algorithm as it uses the theoretical minimum number of fringe patterns for phase-shifting profilometry. To avoid the camera saturation, a dual-camera fringe projection system is built to measure shiny objects from two different directions. The erroneous phase obtained from a saturated pixel is corrected by the phase of its corresponding pixel in the other view which is free from the saturation problem. To achieve high measurement accuracy, the corresponding high light intensity areas in cameras are found by sub-pixel matches of the speckle pattern in either view. Benefited from the trifocal tensor constraint, the corresponding points in the two wrapped phase maps can be directly established, and thus, the difficulties in determining the correct fringe order for the discontinuous or isolated surfaces can be effectively bypassed. Experimental results indicate that the proposed method is able to successfully measure highly reflective surfaces for both stationary and dynamic scenes.

1. Introduction

Fast three-dimensional (3-D) shape measurement is playing an increasingly important role nowadays in many fields including online inspection, rapid inverse engineering, medical sciences and home entertainments. Traditionally, a coordinate measuring machine is often used to inspect contours of objects due to its advantage of high precision. However, its measurement speed is very slow because of the requirement of surface-contacts. In contrast, the image-based optical 3-D measurement is more efficient and free from physical contacts [1,2]. Generally, optical 3-D shape measurements can be classified into passive methods and active methods. To obtain reconstructions of high accuracy, the latter that actively illuminate the measured object with pre-designed light signals are more appealing. Among the active means, fringe projection is one of the most widely used techniques because of its superiorities of high resolution, precision and full-field measurement.

To achieve fast measurements with the fringe projection, some researchers employed Fourier transform profilometry (FTP) [3–6], by which only one fringe pattern is used for 3-D measurements. It can be found that this method is particularly suitable for fast measurements since its sensitivity to object movements has been reduced to the minimum (a single shot). Conventionally, however, this technique is usually adopted for a continuous surface, e.g. a single object without large depth variation. This is because the phase information is solved by a frequency-domain filtering with FTP, the problem of frequency overlap may emerge when a measured surface is of large variation of slope. Owing to rapid developments of digital light projecting and capturing devices, many researchers begin to use the phase shifting profilometry (PSP) by which multiple fringe patterns are utilized [7–12]. As the capturing speed of cameras is increased, the moving process can be assumed as a quasi-static process, which makes the implementations of the multi-pattern strategy possible. More importantly, PSP has advantages of higher precision, resolution and being insensitive to ambient light over FTP. Based on PSP, Wang and Zhang [13] proposed a nine-pattern method to measure moving objects. Then, to reduce the number of used patterns Zuo et al. [14] developed a

* Corresponding author at: Jiangsu Key Laboratory of Spectral Imaging & Intelligent Sense, Nanjing University of Science and Technology, Nanjing, Jiangsu Province 210094, China.
E-mail address: geniusshijie@163.com (S. Feng).

http://dx.doi.org/10.1016/j.optcom.2016.07.057
0030-4018/

fringe projection system by employing five images to reconstruct 3-D shapes of fast rotating blades. Further, Weise et al. [15] and Zhong et al. [16] presented techniques by which only the three fringe patterns were utilized for unambiguous 3-D depth measurements. In their methods, the phase unwrapping was conducted relied on relations resulted from the multi-view geometry. Recently, Feng et al. [17] proposed an approach where only two patterns were used. One of the images is a speckle pattern and the other one is a composite pattern fused by the digital speckles and a fringe pattern. The speckles are used to unambiguously unwrap the phase obtained from the fringe image. For the mentioned methods, although they would show good performance for fast measurements of dynamic scenes, it may be difficult for them to handle the objects with shiny surfaces. For fringe projection techniques the major problem faced when they are used to inspect highly reflective areas is that the 3-D depth sensing is entirely relied on the image processing of captured patterns. Once the image pixel is saturated as a result of the intense reflected light at a highly reflective point, no fringe can be recorded and used for the 3-D shape reconstruction.

Thus to cope with shiny objects, Zhang et al. [18] proposed a high dynamic range measuring technique based on the multi-exposure strategy. By their method, the fringes on the highly reflective surface were obtained by fusing the ones captured at several pre-determined exposure times. A decreased exposure time was used to capture the fringes at shiny points. With the same principle, Waddington and Kofman [19] developed a technique which adjusts the illumination intensity of the projector to avoid the camera saturation. Subsequently, Jiang et al. [20] presented a method that combines both strategies to modify the exposure time of the camera and the projected light intensity simultaneously. Additionally, Feng et al. [21] reported a generic high dynamic range fringe projection method where the required exposure time was adaptively predicted and polarizers were introduced to remove the high intensity. For the above methods, however, they were developed for still objects and thus may not be appropriate for measuring dynamic scenes. For the method by polarization, the reduced intensity by polarizers may result in low signal to noise ratio for captured patterns. For methods based on the image fusion, they need to capture many patterns to synthesize into a single fringe image. Thus, it is difficult for camera pixels to measure unchanged points at different exposures given the movements of the object.

Therefore to handle the highly reflective surface with less patterns, Chen and Zhang [22] proposed to use traditional phase shifting algorithms with several saturated fringe patterns. Compared to multi-exposure methods, their method can perform the measurement with saturated fringes obtained from a fixed exposure time, which greatly reduces the number of required patterns. However, in their method the amount of patterns is proportional to the period of the fringe pattern. Thus to employ less patterns, one needs to reduce the fringe pitch, which may increase the difficulty in phase unwrapping if too narrow fringes are used [23]. Besides, additional patterns are still needed to meet the goal of unambiguous shape measurements. With the same strategy of utilizing saturated fringes, Chen et al. [24] and Hu et al. [25] suggested to use extra phase shifts (more than the minimum) to alleviate the effect of the shiny surface. To better eliminate the influence of the saturation, however, one still need to increase the number of the phase shifts to allow more unsaturated pixels to be used for phase measurements. Then, based on [19] the methods reported in [26,27] use adaptive modification of the illumination intensity of the projected pattern to inspect shiny surfaces. This strategy can provide local shiny areas with required illuminations by projecting adaptive patterns. Compared to the global method [19], the adaptive technique saves the patterns to be projected. But for the generation of adaptive patterns, the measured object should keep static for locations of the highly reflective regions. Thus they may not be suitable for dynamic objects. Moreover, Liu et al. [28] and Kowarschik et al. [29] resorted to the idea of changing the viewing angle to remove the effect of the high light intensity. But, for [28] it needed the multi-exposure technique to obtain an unwrapped phase map for the pixel matching in different views and for [29] the alteration of the viewing angle was achieved by manually modifying the orientation of the measuring platform. Therefore both of them would show difficulties for measurements of dynamic objects.

For the purpose of developing a method for fast measurements of varying highly reflective surfaces, we present a novel fringe projection strategy. In the work, to lower the sensitivity to motions we only employ four patterns among which three images are phase-shifting fringes and the remaining one is an image of digital speckles. The three-step phase-shifting algorithm is applied for the phase measurement. Because of the camera saturation caused by the high light intensity, the obtained phase for the shiny region is prone to be erroneous. Therefore, to correct phase errors we utilize another camera viewing from a different angle to build a stereo fringe projection system. The reason is that when observing from another side the reflected light at a shiny point will not be so strong that saturates the corresponding pixel. Thus the phase from the newly introduced camera can be used to compensate the erroneous phase in the former view. To find the corresponding area in these cameras, we use the speckle image to mark the local region uniquely. To obtain measurement results of high accuracy, we introduce the enhanced normalized cross correlation (ENCC) method [30] into this work to acquire a disparity map with sub-pixel precision. Once phase errors are corrected, the trifocal tensor obtained from the tri-view relation is used to unwrap the phase unambiguously. Experimental results demonstrate that the method can measure objects of highly reflective surface successfully and efficiently.

2. Principles

2.1. Overview of the algorithm

For an intuitive understanding of our method, at the beginning we provide an overview of the approach. As shown in Fig. 1, our method can be performed by four steps, which are represented with different colors. For the first step, we capture the phase-shifting and speckle patterns by both cameras, and rectify all of them based on the results of the stereo-camera calibration. Then, the rectified speckle images from both cameras are employed to find corresponding shiny areas in the two views. By the ENCC, a sub-pixel disparity map indicating the highly reflective areas can be obtained. In the second step, we firstly calculate the wrapped phase maps with the rectified fringe patterns and then conduct the phase error correction for both phase maps with the aid of the sub-pixel disparity map. Next, in the third step, with accurate phase maps from both cameras we can compute the fringe order by the trifocal tensor. In the final step, with the fringe order the wrapped phase maps are unwrapped unambiguously and converted to heights.

2.2. Three-step phase-shifting algorithm

N-step phase-shifting profilometry is a well-known technique for phase measurements. A set of fringe patterns with a certain phase shift is projected cyclically onto a measured scene. From a different position, a camera captures these distorted patterns for 3-D reconstructions. A schematic is shown in Fig. 2. To ensure the

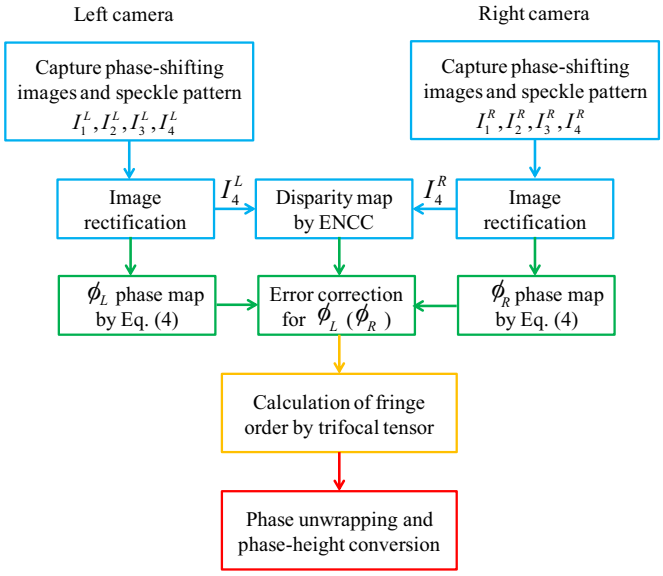

Fig. 1. The flowchart of the proposed method.

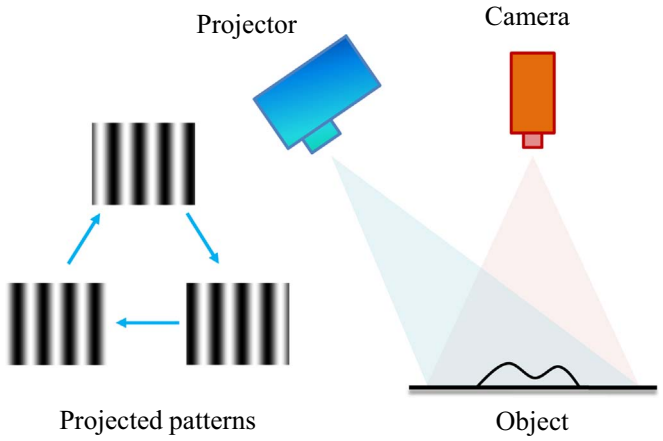

Fig. 2. The schematic of the three-step phase-shifting method.

lowest sensitivity to the object motion, the minimum of three fringe patterns is used in this work. By the three-step phase shifting algorithm, the intensities of the patterns can be expressed by

$$I_1(x, y) = A(x, y) + B(x, y)\cos\left[\phi(x, y) - 2\pi/3\right] \tag{1}$$

$$I_2(x, y) = A(x, y) + B(x, y)\cos\left[\phi(x, y)\right] \tag{2}$$

$$I_3(x, y) = A(x, y) + B(x, y)\cos\left[\phi(x, y) + 2\pi/3\right] \tag{3}$$

where (x,y) is the pixel coordinate, $A(x, y)$ the average intensity that can be obtained by $[I_1(x, y) + I_2(x, y) + I_3(x, y)]/3$ and $B(x, y)$ the phase modulation. $\phi(x, y)$ is the phase that can be calculated by

$$\phi(x, y) = \tan^{-1}\frac{\sqrt{3}\left[I_1(x, y) - I_3(x, y)\right]}{2I_2(x, y) - I_1(x, y) - I_3(x, y)} \tag{4}$$

In general, the intensities of these images should not reach the maximum intensity limit of the camera sensor, e.g. 255 for the 8-bit pixel depth. This is because the camera can no longer capture the variation of intensities for the fringe in this case. However, when inspecting the surface with shiny regions, it is very easy for camera pixels to reach the limit. Consequently, the obtained phase of the highly reflective parts would be erroneous. To show the adverse effect of the camera saturation, we simulate fringe patterns captured from planes with diffuse and highly reflective surfaces, which are shown in Figs. 3(a) and 3(b) respectively. It can be seen that the most area of fringe patterns of the shiny surface is pure white, which indicates that the corresponding camera pixels are saturated. Fig. 3(c) shows the calculated phase distributions of these surfaces. We can find that due to the camera saturation, the phase is recovered with some undesired ripples compared with the normal phase distribution.

2.3. Phase error correction

To address the problem of the camera saturation, we firstly study the surface reflection model which is illustrated in Fig. 4(a). In the model, a surface reflection is composed of three components: a diffuse lobe, a specular spike and a specular lobe. The diffuse lobe, consisting of the light from multiple surface reflections and internal scattering, reflects hemispherically in all directions. The specular lobe distributes in a limited range around the specular spike whose angle of reflection equals to that of incidence. Normally, for a shiny point the intensities of the specular lobe and specular spike are much higher than that of the diffuse lobe. As a result, when a camera (c_1) is positioned by an angle within that specular range, it is likely to be saturated. Thus, intuitively to bypass the camera saturation, the camera would be placed at a position like c_2 for which only the light from the diffuse lobe is captured. While for a specific object, the camera could be placed in a direction which avoids this reflection from saturating the camera. But for different highly reflective samples, the direction of the specular reflection may change due to their different shapes. Hence it is cumbersome to keep changing the camera orientation from sample to sample. The second case would be when an object might have multiple specular reflections in different directions. It is illustrated in Fig. 4(b) in which although the point P_a can be captured with the diffusive light, the image of point P_b is unable to avoid the saturation problem. Therefore to cope with this issue, a dual-camera fringe projection system is built and shown in Fig. 5. Since the specular components only spread in the small angle of observation, it is less likely for the two cameras viewing from different angles to be saturated at the same time for the same measured point. Thus from this newly introduced camera (denoted as right camera), fringe patterns free from the saturation at P_a can be obtained. As long as the desired fringes are acquired, the phase of the right camera can be readily retrieved through Eq. (4).

Since the phase of interest from the right camera is not affected by the shiny area, we can use it to correct the erroneous phase in the left camera. To robustly find the same area in both views, we tend to project a pattern which can be used as a texture for the search of the corresponding highly reflective region. Due to the existence of the high light intensity, it is necessary to design a pattern that is not sensitive to the intense reflected light, which means it can be observed by both cameras. From our observations, we find that the speckle pattern is the one that is immune to the shiny object. This is illustrated in Fig. 6 where a fringe pattern is simulated by a sinusoidal wave and a black and white speckle image by a square wave since the speckle only has two grey scales. Suppose that these patterns are incident onto a highly reflective surface. From the figure, it can be seen that due to the effect of pixel saturation, the actual sinusoidal wave is captured as a trapezoid-shaped pattern. However for the speckle pattern, although its actual intensity is reduced to the maximum allowed intensity, its shape can be well preserved. This feature ensures the spatial

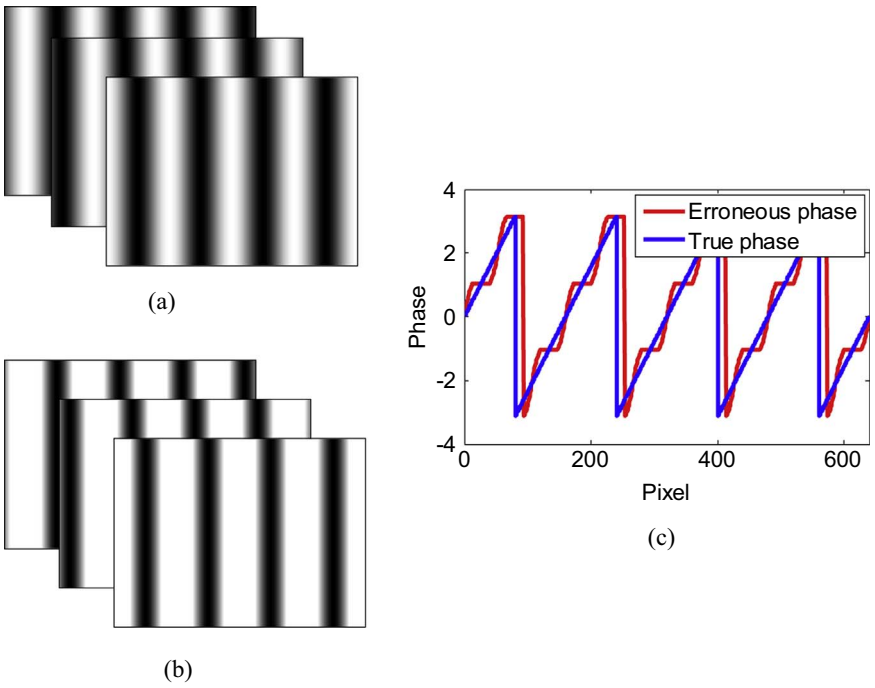

Fig. 3. The effect of the camera saturation on the phase measurement. (a) Simulated fringe patterns captured from a diffuse plane; (b) simulated fringe patterns captured from a shiny plane; (c) cross-sections of the phase maps, where the red line shows the phase influenced by the shiny surface. (For interpretation of the references to color in this figure caption, the reader is referred to the web version of this paper.)

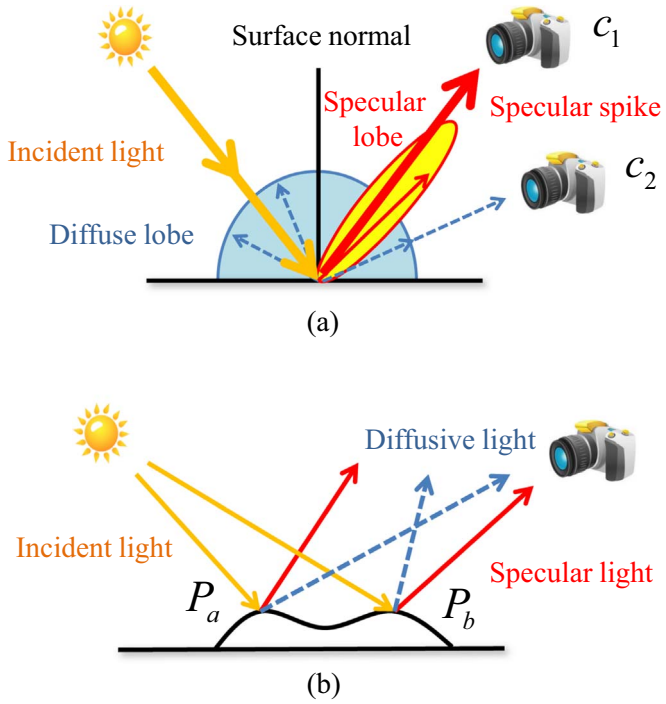

Fig. 4. (a) The surface reflection model; (b) surface reflections with multiple shiny areas.

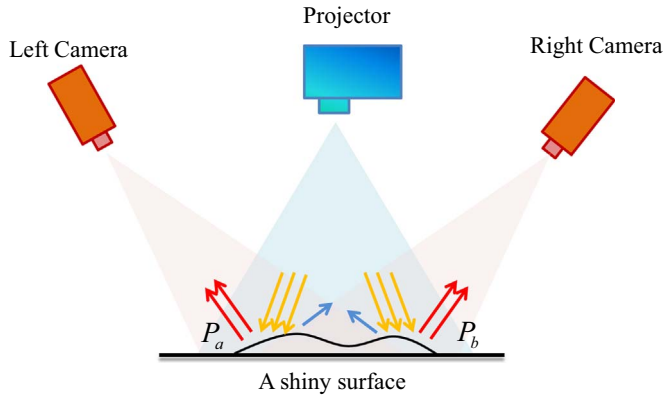

Fig. 5. The schematic of the dual-camera fringe projection system.

invariance for the local distribution of the speckle pattern, which is the key point for the search of the highly reflective area in the two cameras.

To generate a speckle pattern, let $I_4(x, y) \in \{0, 1\}$ be of high distinguishability, it is designed by the following rules [17]: (1) the digital speckle consists of white dots distributed on a black background, and the size of each white dot is $N \times N$ pixels; (2) in each region of equivalent size of 3×3 dots, only a single dot is white; (3) none of any two white dots are adjacent in their eight neighborhoods. For the compensation of the phase errors, the speckle patterns are used to obtain a disparity map $d(x, y)$ which encodes the offset in horizontal coordinates of corresponding image points. Widely adopted measures for similarity are the sum of squared differences, the sum of absolute differences and the normalized cross-correlation (NCC). In general, results from these methods are of accuracy of pixel level. In order to calculate a disparity map more precisely, we introduce the Enhanced Normalized Cross Correlation (ENCC) into our work by which the accuracy can be achieved with sub-pixel level [30]. This method uses a proper interpolation scheme in two adjacent candidate windows of the match image and employs the classical zero mean normalized cross correlation function to measure the similarity. For ENCC, firstly the images from the two cameras need to be rectified, making the search direction horizontally. Then we define $W(x, y)$ is the sub-window image centered at pixel (x,y) of size $N_1 \times N_2$, and let

$$w(x, y) = [w_1 \ w_2 \ \dots \ w_N] \tag{5}$$

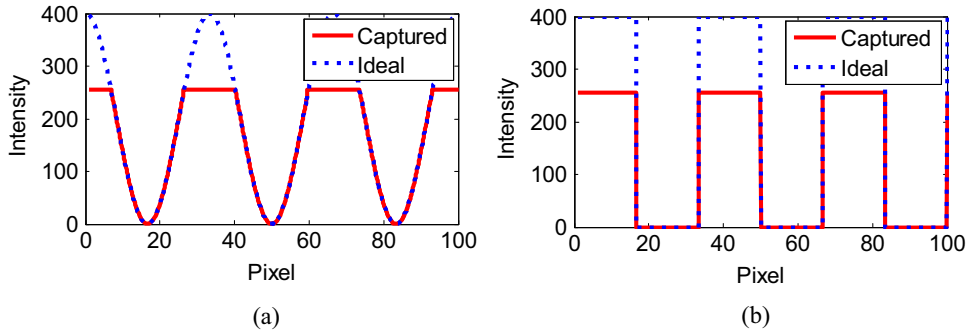

Fig. 6. The effects of the shiny surface on captured patterns. (a) Captured intensity of a fringe pattern; (b) captured intensity of a speckle pattern.

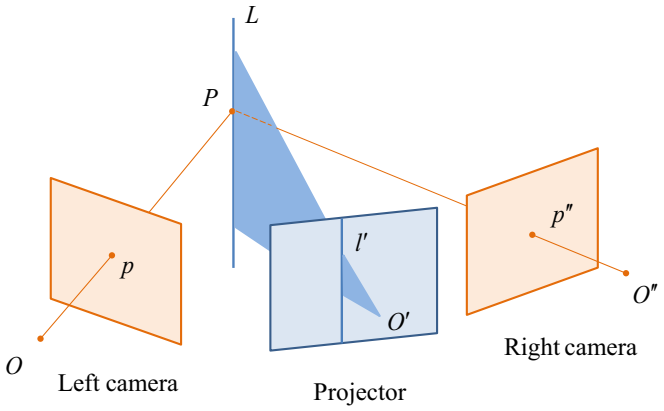

Fig. 7. The schematic of the imaging correspondence of a point in three views.

be the vector by stacking up the columns of the window $W(x, y)$, where $N = N_1N_2$. Then the zero mean normalized vector w^o is defined as

$$w^o(x, y) = \frac{w(x, y) - \bar{w}(x, y)}{\|w(x, y) - \bar{w}(x, y)\|_2} \tag{6}$$

where $\bar{w}(x, y)$ is the mean value and $\|\ \|_2$ the Euclidean norm.

Let d_0 be an integer disparity which corresponds to the maximum correlation coefficient which can be expressed by

$$\rho_{x,y,d_0} = w_L^o(x, y)w_R^o(x, y - d_0) \tag{7}$$

where L and R means the left and right images respectively. Then d_0 can be solved by the following maximization problem:

$$d_0(x, y) = \max_{0<d<D} \rho_{x,y,d} \tag{8}$$

where D is the disparity variation range which is set according to practical situations. To obtain a disparity map $d'(x, y)$ with sub-pixel accuracy, we define a continuous spatial translation parameter τ and $d'(x, y)$ can then be written as

$$d'(x, y) = d_0(x, y) - \tau(x, y) \tag{9}$$

Since $d_0(x, y)$ is obtained by Eq. (8), to evaluate $d'(x, y)$ we solve the maximization of the correlation coefficient as

$$\max_{\tau} w_L^o(x, y)w_R^o(x, y - d_0 + \tau) \tag{10}$$

Finally the coefficient attains its maximum on

$$\tau = \frac{\rho_{d_0-1} - r\rho_{d_0}}{\lambda(r\rho_{d_0-1} - \rho_{d_0}) + r\rho_{d_0} - r\rho_{d_0-1}} \tag{11}$$

where

$$\rho_{d_0}(\tau) = \sqrt{\frac{\rho_{d_0}^2 + \rho_{d_0-1}^2 - 2r\rho_{d_0}\rho_{d_0-1}}{1 - r^2}} \tag{12}$$

$$\lambda = \frac{\|w_R(x, y - d_0 - 1) - \bar{w}(x, y - d_0 - 1)\|_2}{\|w_R(x, y - d_0) - \bar{w}(x, y - d_0)\|_2} \tag{13}$$

$$r = w_R^o(x, y - d_0)w_R^o(x, y - d_0 - 1) \tag{14}$$

The parameter λ is the ratio of norms of the adjacent windows and r their correlation coefficient. These two parameters are used to show the similarity between the windows $w_R(x, y - d_0)$ and $w_R(x, y - d_0 - 1)$. Given the similarity, we can then determine the sub-pixel position between the adjacent pixels by Eq. (11). As we have obtained the disparity map $d'(x, y)$ by Eqs. (9)–(14), the phase error in the left camera can be readily corrected by

$$\phi_L(x, y) = \phi_R(x, y - d') \tag{15}$$

where $\phi_L(x, y)$ and $\phi_R(x, y)$ are the wrapped phase maps corresponding to the left and right camera respectively. (x,y) shows the point that needs to be compensated, which can be located by

$$(x, y) \in \{I_1(x, y) = 255 \cup I_2(x, y) = 255 \cup I_3(x, y) = 255\} \tag{16}$$

where 255 is the saturated intensity. For Eq. (15), because the offset in $d'(x, y)$ is at the sub-pixel level, the calculation of $\phi_R(x, y - d')$ is performed by the bilinear interpolation.

As shown in Fig. 5, the problem of pixel saturation can also occur in the right camera. In this case, the phase from the left camera can be used to correct the phase error in the right view. Therefore to compensate the phase error in the right camera, Eq. (15) can be changed into

$$\phi_R(x, y) = \phi_L(x, y + d') \tag{17}$$

The reason for the compensation of the erroneous phase in the right camera is that for the phase unwrapping method introduced in the coming sub-section, it requires two accurate wrapped phase maps from both views. It is noted that for some objects several shiny points may cause the saturation issue for the same pixels in both camera views. From experiments, it happens only occasionally and will not affect the measurement of the whole surface since the size of this kind of area is very small in general. To alleviate the problem, one can slightly change the position or the orientation of the measured object, or enlarge the viewing angle between the two cameras. When to measure dynamic surfaces, the inherent motions of objects may help avoid the issue of saturation happening in both cameras since the shiny spots are moving over time.

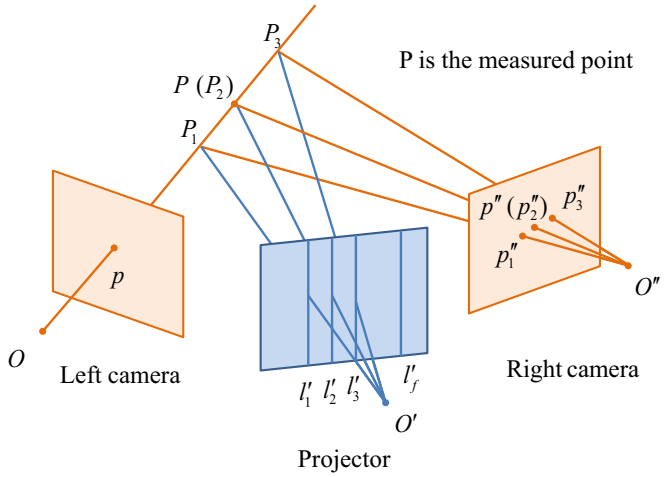

Fig. 8. The one-to-many point correspondences when using multi-frequency fringe patterns.

2.4. Trifocal tensor based fast phase unwrapping

From Eq. (4), we can find that the phase $\phi(x, y)$ solved by the arctan function is actually a principal value which ranges from $[-\pi, \pi]$ with 2π discontinuities. A spatial phase unwrapping is usually employed to remove the phase ambiguity for fast measurements as it does not require additional images. However, as the spatial phase unwrapping is designed to use the phase relationship between neighboring pixels, it tends to fail when detecting the fringe order for the points on the edges of isolated objects. Due to the limitation, temporal phase unwrapping is developed to use more assistant patterns to unwrap the phase. With more images, each pixel is encoded uniquely in the time axis and thus can be unwrapped independently. However, this method may not be very suitable for dynamic measurements since it requires many patterns, which would increase the sensitivity to object motions.

Here to unwrap the phase without introducing extra patterns, we employ the trifocal tensor. By this method, only the wrapped phase maps obtained by Eq. (4) are sufficient to solve the fringe order unambiguously. This is achieved by constraints in the multi-view geometry as shown in Fig. 7. Suppose a point P in 3-D space is imaged by the left and right camera with image points p and p'' respectively. P is also on a space line L whose projection in the image of the projector is l'. According to the imaging relation between three views [31], by the tensor notion this point-line-point correspondence can be expressed by

$$p^i l'^j (p''^k \varepsilon_{kqs}) T_i^{jq} = 0_s \tag{18}$$

where the image points p, p'', and projection line l' can be written as $p = (p^1, p^2, p^3)^T$, $p'' = (p''^1, p''^2, p''^3)^T$, and $l' = (l'^1, l'^2, l'^3)^T$ respectively by homogenous coordinates. T_i^{jq} is the trifocal tensor which constitutes a $3 \times 3 \times 3$ matrix and can be solved by the Gold Standard algorithm [31].

Normally fringe patterns of multiple periods are preferred for a high signal to noise ratio. Thus, for each pixel with a certain wrapped phase value in the left camera, we may obtain several candidate lines and corresponding image points which have the same phase value in the images of the projector and the right camera respectively. This can be illustrated by Fig. 8. Given that the phase of p is ϕ_p. If the fringe pattern has f periods, we can find f vertical lines (vertical fringes are used) in the image of the projector with the same wrapped phase $\phi_{l'_1} = \phi_{l'_2} = \cdots = \phi_{l'_f} = \phi_p$ and their positions can be calculated by

$$y_{l'_i} = \frac{\left[\phi_p + 2\pi(i-1)\right] width}{2\pi f} \tag{19}$$

where $i = 1, 2 \ldots f$ and *width* is the pixel width of the image plane of the projector. For each vertical line l'_i, we can find a corresponding point p''_i in the right camera by Eq. (18). Thus the actual point to find is among the f possible points of p''_i. To determine the desired image point, we can calculate the phase difference between the point p and the candidate p''_i. The ideal p'' is supposed to have the minimum difference because they are viewing the same point in 3-D space. In practice, however, due to the effects of the phase error, occlusions and noises, some false candidate points may have closer phase value to ϕ_p than the real point does. Therefore, to handle this problem a two-step error correction strategy is employed here. For the first step, we can remove some undesired candidates by the knowledge of the measurement range. For example, for a pixel measuring a point moving in a fixed range of depth, its possible fringe order may be in the subset of $[1, 2, \ldots, f'] \subseteq [1, 2, \ldots, f', f'+1, \ldots, f]$. In this case, the candidate points p''_i corresponding to fringe orders $f'+1$ to f can be eliminated. For the second step, we combine the phase difference and the NCC to produce a new measure for the identification of corresponding points since the speckle pattern is locally unique and can be used eliminate false matches. The measure is expressed as

$$M\left[p(x, y), p''_i(x''_i, y''_i)\right] = diff(\phi_p, \phi_{p''_i}) + 1 - \left|NCC(p, p''_i)\right| \tag{20}$$

$$diff(\phi_p, \phi_{p''_i}) = \left|\phi_p - \phi_{p''_i}\right| \tag{21}$$

$$NCC(p, p''_i) = \frac{\sum_{m,n}(Q(m, n) - \bar{Q})(R(m, n) - \bar{R})}{\sqrt{\sum_{m,n}(Q(m, n) - \bar{Q})^2}\sqrt{\sum_{m,n}(R(m, n) - \bar{R})^2}} \tag{22}$$

where Q and R are sub-images centered at $p(x, y)$ and $p''_i(x''_i, y''_i)$ with the size of $m \times n$. The subscript i is an index of the possible candidates of p'' on the image plane of the right camera. The candidate point p''_i with the minimum M is the one to be obtained. Further, in practical measurements the points near the phase jumps of the wrapped phase map may fail to find their corresponding points. Thus, for this case the edge points adjustment can be used to assist identifying the real matching point [16]. As the corresponding point in right image is found, its related projection line of known fringe order in the projector image can be determined readily. Thus the phase at point p can be unwrapped by

$$\Phi_p(x, y) = \phi_p(x, y) + 2\pi f_p \tag{23}$$

where f_p is the fringe order at point p. With the unwrapped phase map, the real-world 3D coordinate can be obtained based on a phase-height conversion algorithm detailed in [17].

3. Experiments

To validate the proposed method, we developed a stereo fringe projection system. It is composed of two high speed cameras (Basler acA640-750um) with resolution of 640×480 and a digital light processing (DLP) light crafter with 608×684 resolution. The synchronization between the units was achieved by the output control signal sent from the light crafter. The used fringe patterns are vertical and of 20 sinusoidal cycles per field of view of 608 pixels. For the generation of the speckle image, N was selected as 1.

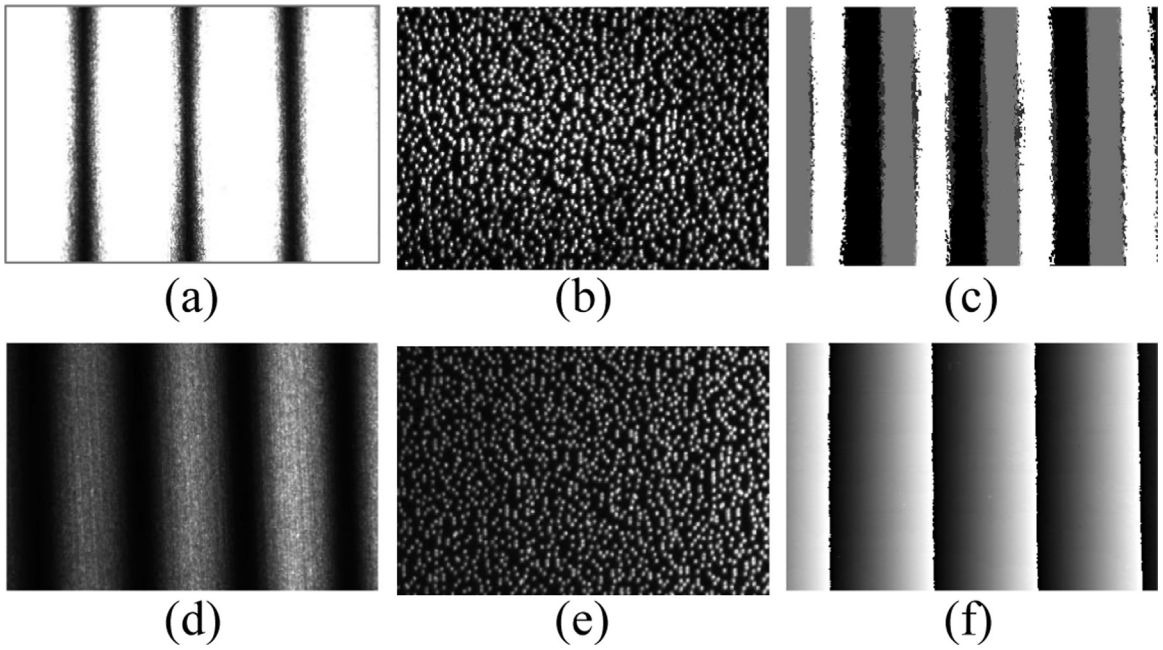

Fig. 9. Experimental images of measuring a work-piece of aluminium alloy. (a) One of the captured fringe patterns from the left camera; (b) the speckle pattern captured by the left camera; (c) solved wrapped phase map without phase error correction; (d) the corresponding fringe pattern recorded by the right camera; (e) the speckle pattern captured by the right camera; (f) compensated phase map with the proposed method.

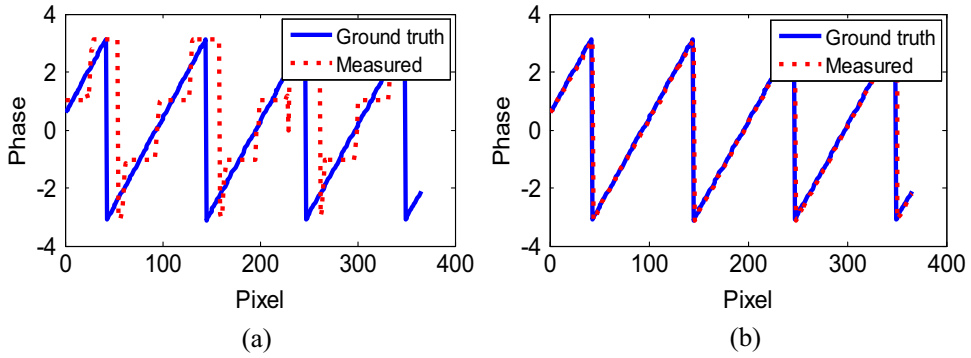

Fig. 10. Phase distributions of the 300th row of the measured object. (a) The result without correction; (b) the result by our method.

To reduce the influence of the high light intensity, a relatively large angle between the two cameras will help avoid capturing images with saturations at the same shiny point. For our setup, the distance between the two cameras was 210 mm and objects to be measured were placed 400 mm away from the system. With this arrangement, the saturation problem was avoided to occur simultaneously for the same pixel in both camera images.

Before measurements, the system was calibrated in two steps. For the first step, 20 images of a black and white checkerboard with different orientations were captured by both cameras. The two cameras were then calibrated by the stereo vision calibration [32]. This step is for the rectification of images captured from the cameras. In the second step, we calculated the trifocal tensor. To find the point correspondence in three views, the projector was treated as an inverse camera. By projecting vertical and horizontal phase-shifting patterns on a reference plane, the position of a point on the image plane of the projector was determined [33]. In the work, we randomly selected 60 points on the reference plane at two different heights ($z=0$ and $z=100$ mm) for the estimation of the trifocal tensor by the Gold Standard algorithm.

3.1. Accuracy evaluation

Firstly we measured a work-piece of aluminium alloy to show the accuracy of the presented method. For comparison, the object was also measured by the traditional multi-exposure technique. The result from the multi-exposure method was regarded as the ground truth. Figs. 9(a) and 9(b) show one of the captured fringe patterns and the speckle image from the left camera. The corresponding images photographed by the right camera are shown in Figs. 9(d) and (e). It can be seen that the measured surface is so shiny that only the darkest regions of the fringes were sensed by the left camera. However, for the speckle pattern all of the speckles can be captured clearly. In the view of the right camera, both the fringes and the speckles have been well preserved. Fig. 9(c) shows the wrapped phase from the left camera calculated by Eq. (4). We can see that the phase distribution is severely distorted because of the saturated pixels. For the correction, we calculated the wrapped phase in the right camera, and by ENCC a disparity map of sub-pixel accuracy was obtained. The erroneous phase was then compensated by Eq. (15) and the result is as shown in Fig. 9(f) where the distortions have been removed completely. In Figs. 10(a) and (b), we plotted the 300th row of the two wrapped

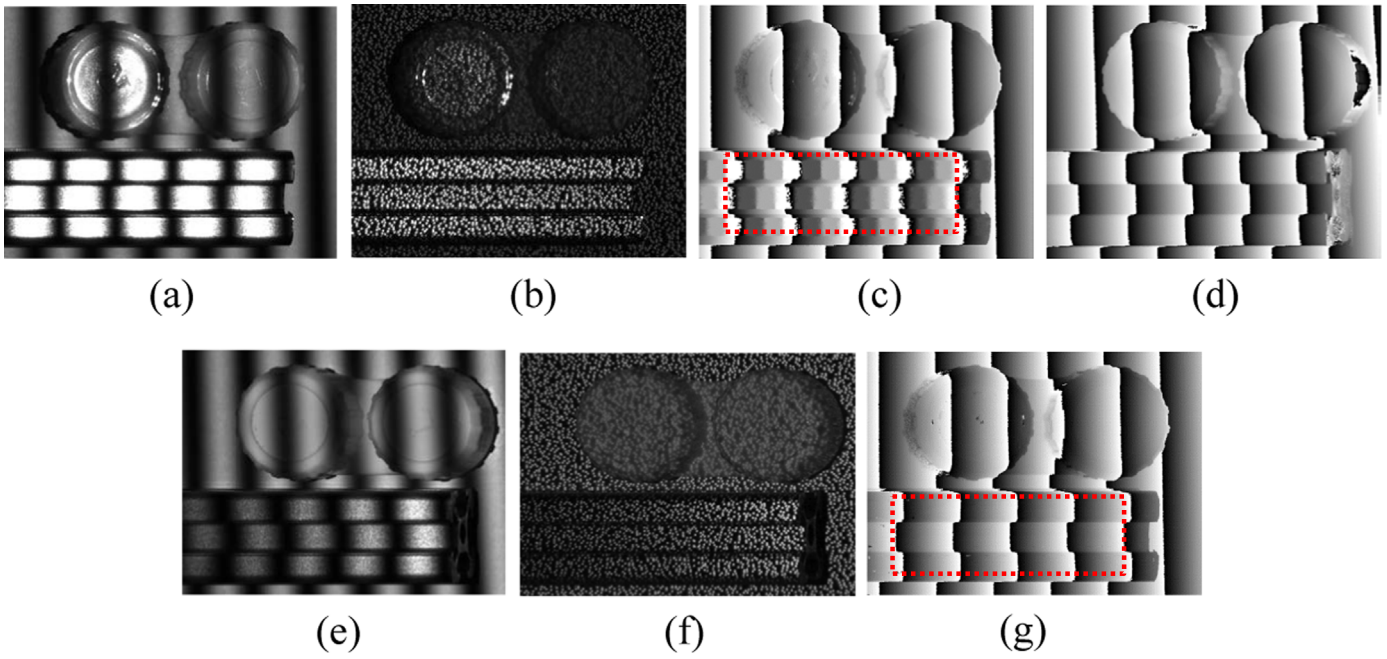

Fig. 11. Measurement images for multiple shiny objects. (a) One of the fringe patterns for the left camera; (b) captured speckle pattern by the left camera; (c) obtained wrapped phase affected by camera saturation; (d) acquired wrapped phase in the right camera; (e) one of the fringe patterns for the right camera; (f) captured speckle pattern by the right camera; (g) corrected phase map with the presented method.

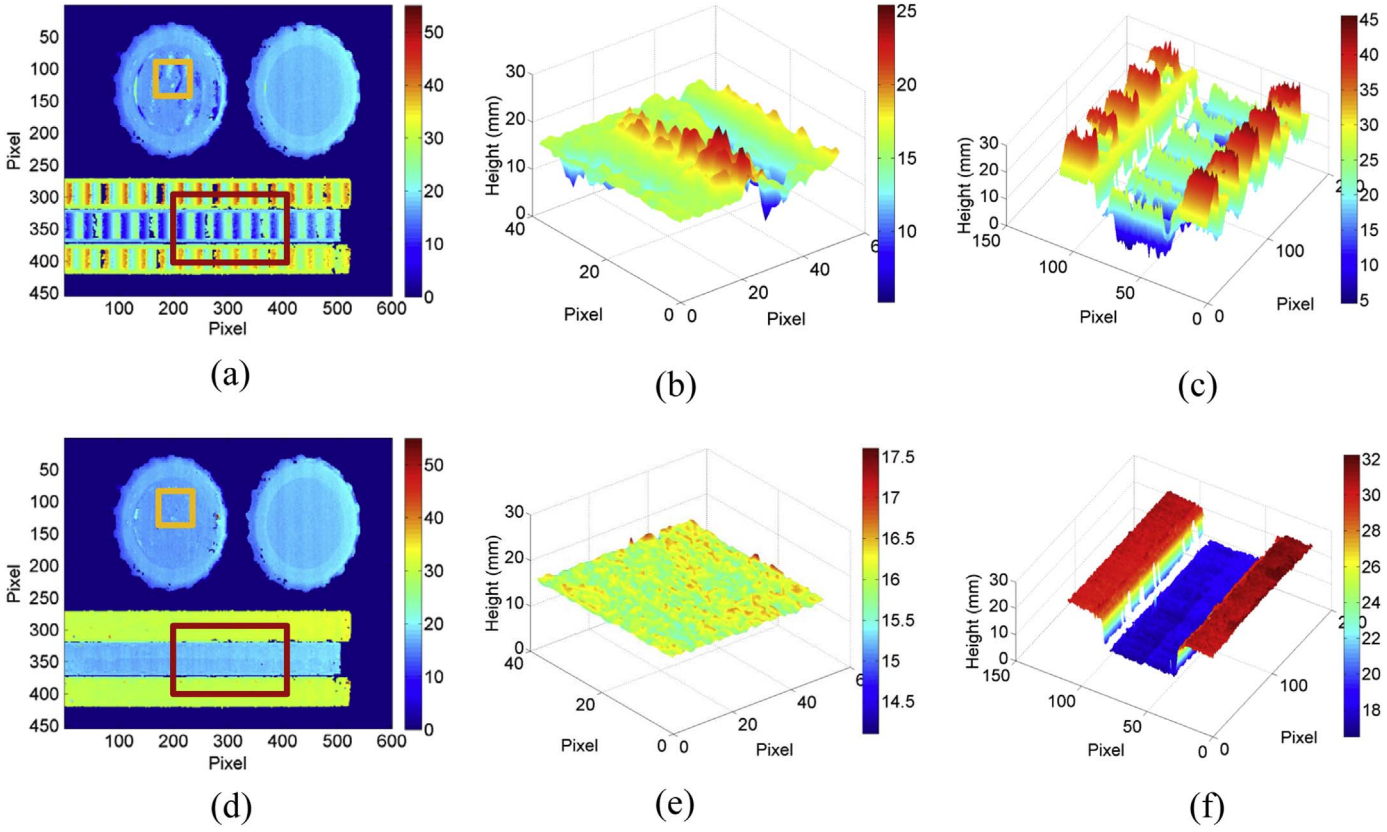

Fig. 12. The comparison of the 3-D reconstruction results. (a) Retrieved 3-D model without error correction; (b) enlarged view of the recovered upper left circular surface in (a); (c) enlarged view of the recovered surface of the work-piece in (a); (d) retrieved 3-D model with our method; (e) enlarged view of the recovered upper left circular surface in (d); (f) enlarged view of the recovered surface of the work-piece in (d).

phase maps. It can be seen that with the presented method the incorrect phase distribution of a contour of steps as shown in Fig. 10 (a) has been corrected effectively compared to the ground truth as shown in Fig. 10(b). Quantitatively, without the correction, for the plotted cross-section the average error is 1.3208 rad and the standard deviation 1.9755 rad. With our method, the average error and the standard deviation have been reduced to 0.0748 rad and 0.0523 rad respectively.

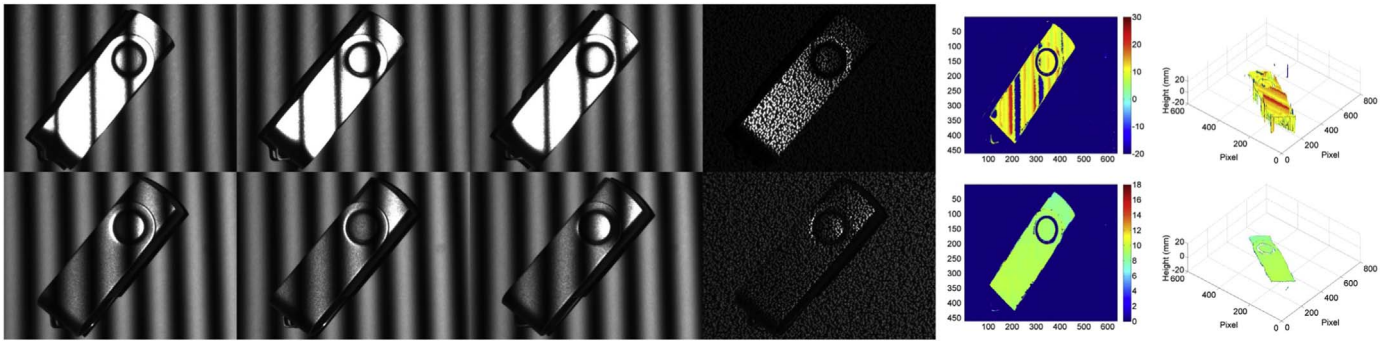

Fig. 13. A screenshot of the measurement video.

3.2. Static objects measurement

Next we tested a scene composed of multiple objects. The objects have shiny surfaces of aluminium alloy and plastic, as can be seen from Fig. 11(a) which is one of the fringe patterns captured by the left camera. The wrapped phase was obtained by Eq. (4) and is shown by Fig. 11(c). Within the dotted rectangle, we can clearly observe that the phase of the aluminium alloy work-piece is very unsmooth because of the phase errors with an appearance of small abrupt squares. When using the proposed method, we captured the fringe pattern from the right camera as shown in Fig. 11(e) and speckle patterns from both angles as shown in Figs. 11(b) and (f). From Fig. 11(e), the fringes of shiny areas of the upper left circular surface and the work-piece have been recorded without any saturated pixels compared with Fig. 11(a). From Fig. 11(b), the speckle pattern was also captured with distinct local features. To compensate the phase error in Fig. 11(c), a disparity map was firstly obtained by ENCC with a sub-window of 9×9 pixels. Then with the disparity map and a phase map solved from the right camera (Fig. 11(d)), Eq. (15) was employed to correct the erroneous phase. Fig. 11(g) shows the compensated result where we can see that on the surface of the work-piece former phase errors with shapes of squares have been successfully eliminated. With the corrected phase, we unwrapped it by the calibrated trifocal tensor and converted the phase to height. Figs. 12(a) and 12(d) show the 3-D reconstructions with and without the proposed method respectively. For a detailed comparison, results of two representative highly reflective regions were selected and enlarged. It can be seen that the fluctuated height distributions on shiny regions of the plastic and aluminium alloy have been changed to smooth surfaces by our method. Although in this experiment there is only one camera being saturated by shiny areas, the proposed technique is competent for the measurement where both cameras are saturated partially since the two cameras can compensate phase errors mutually by Eqs. (15) and (17). This experiment shows the capability of the proposed method to measure a stationary scenario involving discontinuous and highly reflective surfaces.

3.3. Dynamic measurement

To show the method's performance of inspecting dynamic scenes, we measured a rotating thumb drive with a shiny cover. Here the measurement system was working at 120 FPS. For the experiment, we firstly recorded the moving process and then retrieved the surface off-line. A video of the measurement and a corresponding screenshot are shown in the video and Fig. 13, respectively. The pseudo color was employed to represent the variation of the height. To show the improvement, in the video we also compared our result with the one without any error compensation, which is shown by the last two windows in the first row. In Fig. 13, we can see that the reflection is very intense and the shiny area nearly covers the whole surface of the thumb drive. From the video, during the rotation most regions of the object are still saturated as can be observed in the first row. When another camera was introduced to capture the images from the right side, the problem of the pixel saturation was greatly avoided as can be seen in the second row. From the results by the proposed method shown in the last two windows in the second row, the highly reflective thumb drive was correctly measured while it was rotating.

4. Conclusion

In this work, we present a novel technique for fast 3-D measurements of moving shiny objects by the fringe projection technique. In order to achieve a low sensitivity towards object motions, four patterns are designed to efficiently obtain a frame of 3-D reconstruction. Three of the images are phase-shifted fringe patterns and the last one is a digital speckle image. The fringes are used to calculate the phase by the three-step phase shifting method. Due to the pixel saturation resulted from highly reflective surfaces, the phase obtained for these regions tends to be erroneous. To correct the phase errors, a dual-camera fringe projection system is built where a new camera is introduced to measure the phase from a different angle. To find the corresponding shiny point in both views, the speckle images are employed as their local distributions are not affected by the pixel saturation. The ENCC method is adopted to obtain a disparity map with sub-pixel accuracy for the phase correction. Again with the aid of stereo cameras, the phase map is unwrapped unambiguously by the trifocal tensor. Experiments show the validity of the method for both stationary and dynamic scenes.

Due to the employment of two cameras, however, the issue of occlusion should be considered when using the presented technique. This is because the phase correction and unwrapping may compromise when a measured point only appears in one camera and is occluded in the other. Thus in this case, adjustments to the measured scene or to the system configuration are preferred. In the future, our work will focus on how to reduce the impacts of the occlusion.

Acknowledgment

This work was financially supported by the China Scholarship Council (No. 201506840058) and the National Natural Science Fund of China (NSFC) (No. 11574152, No. 61505081, No. 61377003).

Appendix A. Supplementary material

Supplementary data associated with this paper can be found in the online version at http://dx.doi.org/10.1016/j.optcom.2016.07.057.

References

[1] F. Chen, G.M. Brown, M. Song, Overview of three-dimensional shape measurement using optical methods, Opt. Eng. 39 (1) (2000) 10–22, http://dx.doi.org/10.1117/1.602438.

[2] S.S. Gorthi, P. Rastogi, Fringe projection techniques: whither we are?, Opt. Lasers Eng. 48 (IMAC-REVIEW-2009-001) (2010) 133–140.

[3] Q. Zhang, X. Su, High-speed optical measurement for the drumhead vibration, Opt. Express 13 (8) (2005) 3110–3116, http://dx.doi.org/10.1364/OPEX.13.003110, URL ⟨http://www.opticsexpress.org/abstract.cfm?URI=oe-13-8-3110⟩.

[4] X. Su, Q. Zhang, Dynamic 3-d shape measurement method: a review, Opt. Lasers Eng. 48 (2) (2010) 191–204, http://dx.doi.org/10.1016/j.optlaseng.2009.03.012, URL ⟨http://www.sciencedirect.com/science/article/pii/S014381660900075X⟩.

[5] M. Takeda, K. Mutoh, Fourier transform profilometry for the automatic measurement of 3-d object shapes, Appl. Opt. 22 (24) (1983) 3977–3982, http://dx.doi.org/10.1364/AO.22.003977, URL ⟨http://ao.osa.org/abstract.cfm?URI=ao-22-24-3977⟩.

[6] Q. Kemao, Two-dimensional windowed Fourier transform for fringe pattern analysis: principles, applications and implementations, Opt. Lasers Eng. 45 (2) (2007) 304–317, http://dx.doi.org/10.1016/j.optlaseng.2005.10.012, URL ⟨http://www.sciencedirect.com/science/article/pii/S0143816606000455⟩.

[7] L. Huang, C. Seng Ng, A. Krishna Asundi, Fast full-field out-of-plane deformation measurement using fringe reflectometry, Opt. Lasers Eng. 50 (4) (2012) 529–533, http://dx.doi.org/10.1016/j.optlaseng.2011.05.006, URL ⟨http://www.sciencedirect.com/science/article/pii/S0143816611001539⟩.

[8] P.S. Huang, C. Zhang, F.-P. Chiang, High-speed 3-d shape measurement based on digital fringe projection, Opt. Eng. 42 (1) (2003) 163–168, http://dx.doi.org/10.1117/1.1525272.

[9] Z. Zhang, C.E. Towers, D.P. Towers, Time efficient color fringe projection system for 3d shape and color using optimum 3-frequency selection, Opt. Express 14 (14) (2006) 6444–6455, http://dx.doi.org/10.1364/OE.14.006444, URL ⟨http://www.opticsexpress.org/abstract.cfm?URI=oe-14-14-6444⟩.

[10] L. Huang, C.S. Ng, A.K. Asundi, Dynamic three-dimensional sensing for specular surface with monoscopic fringe reflectometry, Opt. Express 19 (13) (2011) 12809–12814, http://dx.doi.org/10.1364/OE.19.012809, URL ⟨http://www.opticsexpress.org/abstract.cfm?URI=oe-19-13-12809⟩.

[11] Y. Zhang, Z. Xiong, F. Wu, Unambiguous 3d measurement from speckle-embedded fringe, Appl. Opt. 52 (32) (2013) 7797–7805, http://dx.doi.org/10.1364/AO.52.007797, URL ⟨http://ao.osa.org/abstract.cfm?URI=ao-52-32-7797⟩.

[12] Z.H. Zhang, Review of single-shot 3d shape measurement by phase calculation-based fringe projection techniques, Opt. Lasers Eng. 50 (8) (2012) 1097–1106, http://dx.doi.org/10.1016/j.optlaseng.2012.01.007, URL ⟨http://www.sciencedirect.com/science/article/pii/S0143816612000085⟩.

[13] Y. Wang, S. Zhang, Superfast multifrequency phase-shifting technique with optimal pulse width modulation, Opt. Express 19 (6) (2011) 5149–5155, http://dx.doi.org/10.1364/OE.19.005149, URL ⟨http://www.opticsexpress.org/abstract.cfm?URI=oe-19-6-5149⟩.

[14] C. Zuo, Q. Chen, G. Gu, S. Feng, F. Feng, R. Li, G. Shen, High-speed three-dimensional shape measurement for dynamic scenes using bi-frequency tripolar pulse-width-modulation fringe projection, Opt. Lasers Eng. 51 (8) (2013) 953–960, http://dx.doi.org/10.1016/j.optlaseng.2013.02.012, URL ⟨http://www.sciencedirect.com/science/article/pii/S0143816613000754⟩.

[15] T. Weise, B. Leibe, L.V. Gool, Fast 3d scanning with automatic motion compensation, in: IEEE Conference on Computer Vision and Pattern Recognition, 2007, CVPR '07, pp. 1–8. http://dx.doi.org/10.1109/CVPR.2007.383291.

[16] K. Zhong, Z. Li, Y. Shi, C. Wang, Y. Lei, Fast phase measurement profilometry for arbitrary shape objects without phase unwrapping, Opt. Lasers Eng. 51 (11) (2013) 1213–1222, http://dx.doi.org/10.1016/j.optlaseng.2013.04.016, URL ⟨http://www.sciencedirect.com/science/article/pii/S0143816613001371⟩.

[17] S. Feng, Q. Chen, C. Zuo, Graphics processing unit assisted real-time three-dimensional measurement using speckle-embedded fringe, Appl. Opt. 54 (22) (2015) 6865–6873, http://dx.doi.org/10.1364/AO.54.006865, URL ⟨http://ao.osa.org/abstract.cfm?URI=ao-54-22-6865⟩.

[18] S. Zhang, S.-T. Yau, High dynamic range scanning technique, Opt. Eng. 48 (3) (2009) 033604–033604-7, http://dx.doi.org/10.1117/1.3099720.

[19] C. Waddington, J. Kofman, Sinusoidal fringe-pattern projection for 3-d surface measurement with variable illuminance, in: 2010 International Symposium on Optomechatronic Technologies (ISOT), 2010, pp. 1–5. http://dx.doi.org/10.1109/ISOT.2010.5687389.

[20] H. Jiang, H. Zhao, X. Li, High dynamic range fringe acquisition: a novel 3-d scanning technique for high-reflective surfaces, Opt. Lasers Eng. 50 (10) (2012) 1484–1493, http://dx.doi.org/10.1016/j.optlaseng.2011.11.021, URL ⟨http://www.sciencedirect.com/science/article/pii/S0143816612000978⟩.

[21] S. Feng, Y. Zhang, Q. Chen, C. Zuo, R. Li, G. Shen, General solution for high dynamic range three-dimensional shape measurement using the fringe projection technique, Opt. Lasers Eng. 59 (2014) 56–71, http://dx.doi.org/10.1016/j.optlaseng.2014.03.003, URL ⟨http://www.sciencedirect.com/science/article/pii/S0143816614000633⟩.

[22] B. Chen, S. Zhang, High-quality 3d shape measurement using saturated fringe patterns, Opt. Lasers Eng. http://dx.doi.org/10.1016/j.optlaseng.2016.04.012. URL ⟨http://www.sciencedirect.com/science/article/pii/S0143816616300458⟩.

[23] C. Zuo, L. Huang, M. Zhang, Q. Chen, A. Asundi, Temporal phase unwrapping algorithms for fringe projection profilometry: a comparative review, Opt. Lasers Eng. 85 (2016) 84–103, http://dx.doi.org/10.1016/j.optlaseng.2016.04.022, URL ⟨http://www.sciencedirect.com/science/article/pii/S0143816616300653⟩.

[24] Y. Chen, Y. He, E. Hu, Phase deviation analysis and phase retrieval for partial intensity saturation in phase-shifting projected fringe profilometry, Opt. Commun. 281 (11) (2008) 3087–3090.

[25] E. Hu, Y. He, W. Wu, Further study of the phase-recovering algorithm for saturated fringe patterns with a larger saturation coefficient in the projection grating phase-shifting profilometry, Optik-Int. J. Light Electron Opt. 121 (14) (2010) 1290–1294.

[26] D. Li, J. Kofman, Adaptive fringe-pattern projection for image saturation avoidance in 3d surface-shape measurement, Opt. Express 22 (8) (2014) 9887–9901, http://dx.doi.org/10.1364/OE.22.009887, URL ⟨http://www.opticsexpress.org/abstract.cfm?URI=oe-22-8-9887⟩.

[27] C. Waddington, J. Kofman, Camera-independent saturation avoidance in measuring high-reflectivity-variation surfaces using pixel-wise composed images from projected patterns of different maximum gray level, Opt. Commun. 333 (2014) 32–37.

[28] G.-h. Liu, X.-Y. Liu, Q.-Y. Feng, 3d shape measurement of objects with high dynamic range of surface reflectivity, Appl. Opt. 50 (23) (2011) 4557–4565.

[29] R. Kowarschik, P. Ku, W. Schreiber, G. Notni, Adaptive optical three-dimensional measurement with structured light, Opt. Eng. 39 (1) (2000) 150–158.

[30] E.Z. Psarakis, G.D. Evangelidis, An enhanced correlation-based method for stereo correspondence with subpixel accuracy, in: Tenth IEEE International Conference on Computer Vision, 2005, ICCV 2005, vol. 1, 2005, pp. 907–912. http://dx.doi.org/10.1109/ICCV.2005.33.

[31] R. Hartley, A. Zisserman, Multiple View Geometry in Computer Vision, Cambridge University Press, Cambridge, 2003.

[32] J.-Y. Bouguet, 2004. Camera Calibration Toolbox for Matlab.

[33] S. Zhang, P.S. Huang, Novel method for structured light system calibration, Opt. Eng. 45 (8) (2006) 083601–083601-8, http://dx.doi.org/10.1117/1.2336196.